Inventory of Supplementary Material for Yuan et al.

Supplementary methods and references are provided that give a more detailed explanation of the modeling that was done in the paper.

Figure 2: The apoptosome-prodomain map.
See **Figure S1** for resolution tests on the final 3D map.

Figure 3: HD2 within the arm of the apoptosome.
See **Figures S2** and **S3** for a sequence/structure diagram for the N-terminal half of Apaf-1 and the fit of other domains in the map. **Table S1** provides fitting cross-correlation values for domains in the map.

Figure 4: The global fit of Apaf-1 and cytochrome c within "active" and ground state apoptosome 3D maps.
See **Figures S4** and **S5** for additional views of the apoptosome model and subunit interface.

Figure 6: Critical interactions in the heptameric platform.
See **Figures S7** and **S8** for further details of the tandem 7- and 8-blade β-propeller modeling and fit in the map.

Figure 7: Assembly of the human apoptosome.

See **Table S2** and **Figure S9** for a summary of NOD mutations that effect apoptosome assembly and function.

Structure of an apoptosome-procaspase-9 CARD complex

Supplemental Online Material- Methods, Tables (2) and Figures (9)

Running title: Structure of an apoptosome-prodomain complex

[+]Shujun Yuan, [+]Xinchao Yu, [¶]Maya Topf, [†] Steven J. Ludtke, [*]Xiaodong Wang and [@+]Christopher W. Akey

[+] Department of Physiology and Biophysics
Boston University School of Medicine
700 Albany St.
Boston, Massachusetts 02118-2526, USA

[*] National Institute of Biological Sciences,
Zhongguancun Life Sciences Park,
Beijing, China

[¶] Institute of Structural and Molecular Biology
Crystallography, Department of Biological Sciences
Birkbeck, University of London
Malet Street
London WC1E 7HX

[†] National Center for Macromolecular Imaging
Verna and Marrs McLean Department of Biochemistry and Molecular Biology
Baylor College of Medicine
1 Baylor Plaza,
Houston, Texas, 77030, USA

[@]Corresponding author: cakey@bu.edu

Supplemental Methods

Molecular modeling of Apaf-1

The sequence of Apaf-1 can be divided into three parts (UniProt accession number: O14727): the N-terminal caspase recruitment domain (CARD), a central nucleotide-binding oligomerization domain (NOD) with helix domain 2 (HD2), and multiple WD40 repeats at the C-terminal region (Acehan et al., 2002, Riedl et al., 2005). A crystal structure in an ADP-bound form (1Z6T) is known for the first 591 residues, which can be divided into 5 domains: CARD (residues 1-89), NBD domain (residues 106-281), Helical Domain 1 (HD1, residues 286-347), Winged-Helix Domain (WHD, residues 361-450), and Helical Domain 2 (HD2, residues 452-586) (Riedl et al., 2005). To gain more insight into the structure of dATP-bound Apaf-1, we generated a pseudo-atomic model that is compatible with our cryo-EM map. We started by docking residues 106-586 from the crystal structure into the density of one of the seven Apaf-1 subunits (α8 linker helix, NBD, HD1, WHD, and HD2) using UCSF Chimera (Pettersen et al 2004). When examining the docked structure, it became clear that NBD, HD1, WHD, and HD2 displayed significant domain rearrangements in the EM structure with respect to the crystal structure. To improve the initial fit, we docked each of the NBD-HD1 and WHD-HD2 domain pairs as a rigid body into the cryo-EM density, followed by a local refinement of the individual domains. Next, the HD1-WHD linker was generated based on the crystal structure of CED-4/CED-9 complex (2A5Y; Yan et al., 2005) using MODELLER-9v7.

For the C-terminal regulatory region of Apaf-1, we applied remote homology detection to residues 592-1249 using HHpred (Söding et al., 2005) and LOMETS (Wu and Zhang, 2007) in combination with PSIPRED secondary structure prediction (Jones, 1999). Our analysis revealed 15 WD40 repeats, most likely arranged as consecutive 7- and 8-blade β-propellers (P7 and P8, respectively). Based on our analysis, we predict that the first strand in the sequence is likely to be the d-strand inserted in the last blade of P8. The sequence then continues into a linker to P7, which is followed by a second linker back to P8 (**Figure S8**). A similar topology was seen in two 7-blade β-propeller domains of yeast Actin Interacting Protein 1 (AIP1, 1PGU). Homology models of the two propellers were built separately based on HHpred alignments, using

MODELLER-9v7 (Sali and Blundell, 1993). Due to a lack of homology, we could not generate reliable models for the two linkers between P7 and P8, and therefore left them unconnected. We docked the homology models of the two β-propellers into the corresponding density in the regulatory region of each Apaf-1 subunit. The search for the correct fit, which was performed by a local rigid fitting with Chimera, included both "flip orientations" of each propeller and the 7 and 8 possible in-plane rotations, respectively. The final fit corresponds to the following arrangement: the bases of the two propellers facing each other, with blades 1 and 7 of P7 positioned in proximity to 8 and 1 of P8, respectively. Bovine-heart cytochrome c (2B4Z, 90% identical to human cytochrome c; Mirkin et al., 2008) was then fitted into the remaining density, between the two β-propellers.

Finally, the entire model was refined with Flex-EM (Topf et al., 2008), to optimize the position of non-hydrogen atoms with respect to their cross-correlation with the map, as well as stereochemical properties and non-bonded interactions, using a conjugate gradient minimization and simulated annealing, molecular dynamics. The optimization was performed hierarchically, such that initially each domain was treated as a rigid body, while atoms in linkers connecting the domains were treated individually, and as the optimization progressed some flexibility was allowed between sub-domains. However, due to the limited resolution the movement of individual secondary structure elements was not allowed in most cases. The cross-correlation coefficient of the final model within the map was 0.91 using Chimera.

Supplemental References

Acehan, D., Jiang, X., Morgan, D.G., Heuser, J.E., Wang, X., and Akey C.W. (2002). Three-dimensional structure of the apoptosome: implications for assembly, procaspase-9 binding and activation. Mol. Cell. 9, 423-432.

Jones, D.T. (1999). Protein secondary structure prediction based on position-specific scoring matrices. J. Mol. Biol. 292, 195-202.

Mirkin, N., Jaconcic, J., Stojanoff, V. and Moreno, A. (2008). High resolution X-ray crystallographic structure of bovine heart cytochrome c and its application to the design of an electron transfer biosensor. Proteins 70, 83-92.

Pettersen, E.F., Goddard, T.D., Huang, C.C., Couch, G.S., Greenblatt, D.M., Meng, E.C. and Ferrin, TE. (2004). J UCSF Chimera--a visualization system for exploratory research and analysis. Comput Chem. 1605-1612.

Riedl, S.J., Li, W., Chao, Y., Schwarzenbacher, R. and Shi, Y. (2005). Structure of the apoptotic protease-activating factor 1 bound to ADP. Nature 434, 926-933.

Sali, A. and Blundell, T.L. (1993). Comparative protein modelling by satisfaction of spatial restraints. J. Mol. Biol. 234, 779-815.

Söding, J., Biegert, A. and Lupas, A.N. (2005). The HHpred interactive server for protein homology detection and structure prediction. Nucleic Acids Res. 33(Web Server issue):W244-248.

Topf, M., Lasker, K., Webb, B., Wolfson, H., Chiu, W. and Sali, A. (2008) Protein structure fitting and refinement guided by CryoEM density. Structure 16, 295-307.

Wu, S. and Zhang, Y. (2007). LOMETS: a local meta-threading-server for protein structure prediction. Nucleic Acids Res. 35, 3375-3382.

Yan, N., Chai, J., Lee, E.S., Gu, L., Liu, Q., He, J., Wu, J.W., Kokel, D., Li, H., Hao, Q., Xue, D. and Shi, Y. (2005). Structure of the CED-4-CED-9 complex provides insights into programmed cell death in Caenorhabditis elegans. Nature 437, 831-837.

Supplemental Tables

Table S1. Cross-correlation values for Apaf-1 domains docked into the map of the apoptosome-pc-9 CARD complex using CHIMERA "Fit in Map".

	NBD	HD1	WHD	HD2	7-blade β-propeller	8-blade β-propeller	cytochrome c	all subunits
CCF	0.853	0.904	0.880	0.920	0.931	0.934	0.949	0.909

Table S2. Summary of NOD protein mutations.

Protein	Mutation	Position in Figure 10	Loss/Gain of function	Region affected §	References
Apaf-1	Apaf-1L		None	Linker between CARD and NBD (aa 99-109 omitted)	Saleh et al., 1999
	Apaf-1-ALT	1	Loss of function	WHD (missing WHD and β-propellers)	Ogawa et al., 2003
	L415P	2	Loss of function	WHD (helix α23 is broken)	Harlan et al., 2006
	437ter	3	Loss of function	WHD (missing helix α24)	Harlan et al., 2006
CED-4	CED-4L	4	Loss of function	NBD (ISM helix)	Shaham et al., 1996
Dark	V316I	5	Loss of function	HD1 (helix α18 region)	Srinvastava et al., 2007
	D333Q	6	Loss of function	HD1 (helix α18 region)	Srinvastava et al., 2007
	A336T	7	Loss of function	HD1 (helix α18 region)	Srinvastava et al., 2007
NOD2	C333Y	8	Loss of function	NBD (ISM helix)	Tanabe et al., 2004
	S344T	9	Loss of function	NBD (ISM helix)	Tanabe et al., 2004
	L348V	10	Loss of function	NBD (ISM helix)	Hugot et al., 2001
	H352R	11	Loss of function	NBD (ISM helix)	Hugot et al., 2001
	V492E	12	Loss of function	HD1 (helix α18 region)	Tanabe et al., 2004
	D382E	13	Gain of function	NBD (Walker B motif)	van Duist et al., 2005
	E383K	13	Gain of function	NBD (Walker B motif)	van Duist et al., 2005
	R334Q	8	Gain of function	NBD (ISM helix)	Miceli-Richard et al., 2001
	R334W	8	Gain of function	NBD (ISM helix)	Miceli-Richard et al., 2001
NLRP3	D303G	13	Gain of function	NBD (Walker B motif)	Danot et al., 2009
	D303N	13	Gain of function	NBD (Walker B motif)	Yu et al., 2006
	R260W	8	Gain of function	NBD (ISM helix)	Yu et al., 2006

§ Apaf-1 nomenclature is used.

References for mutation studies-

Danot, O., Marquenet, E., Vidal-Ingigliardi, D. and Richet, E. (2009). Wheel of life, wheel of death: a mechanistic insights into signaling by STAND proteins. Structure. 17, 172-182.

Harlan, J., Chen, Y., Gubbins, E., Mueller, R., Roch, J-M, Walter, K., Lake, M., Olsen, T., Metzger, P., Dorwin, S., Ladror, U., Egan, D.A., Severin, J., Johnson, R.W., Holzman, T.F., Voelp, K., Dacenport, C., Beck, A., Potter, J., Gopalakrishnan, M., Hahn, A., Spear, B.B., Halbert, D.N., Sullivan, J.P., Abkevich, V., Neff, C.D., Skolnick, M.H., Shattuck, D. and Katz, D.A. (2006). Variants in Apaf-1 segregating with major depression promote apoptosome function. Mol. Psychiatry. 11, 76-85

Hugot, J.-P., Chamaillard, M., Zouali, H., Lesage, S., Cezard, J.-P., Belaiche, J., Almer, S., Tysk, C., O'Morain, C.A., Gassull, M., Binder, V., Finkel, Y., Cortot, A., Modigliani, R., Laurent-Puig, P., Gower-Rousseau, C., Macry, J., Colombel, J.-F., Sahbatou, M., Thomas, G. (2001). Association of NOD2 leucine-rich repeat variants with susceptibility to Crohn's disease. Nature. 411, 599-603.

Miceli-Richard C., Lesage S., Rybojad M., Prieur A.M., Manouvrier-Hanu S., Hafner R., Chamaillard M., Zouali H., Thomas G., Hugot J.-P. (2001). CARD15 mutations in Blau syndrome. Nat. Genet. 29, 19-20.

Ogawa, T., Shiga, K., Hashimoto, S., Kobayashi, T., Horii, A., Furukawa, T. (2003). PAF-1-ALT, a novel alternative splicing form of APAF-1, potentially causes impeded ability of undergoing DNA damage-induced apoptosis in the LNCaP human prostate cancer cell line. Biochem. Biophys. Res. Commun. 306, 537-543

Saleh, A., Srinivasula, S.M., Acharya, S., Fishel, R., Alnemri, E.S. (1999). Cytochrome c and dATP-mediated oligomerization of Apaf-1 is a prerequisite for procaspase-9 activation. J. Biol. Chem. 274, 17941-17945.

Shaham S., Horvitz H.R. (1996). An alternatively spliced C. elegans ced-4 RNA encodes a novel cell death inhibitor. Cell 86, 201-208.

Srinvastava, M., Scherr, H., Lackey, M., Xu, D., Chen, Z., Lu, J. and Bergmann, A. (2007). ARK, the Apaf-1 related killer in Drosophila, requires diverse domains for its apoptotic activity. Cell Death Differ. 14, 92-102.

Tanabe, T., Chamaillard, M., Ogura, Y., Zhu, L., Qiu, S., Masumoto, J., Ghosh, P., Moran, A., Predergast, M.M., Tromp, G., Williams, C.J., Inohara, N. and Nuñez, G. (2004). Regulatory regions and critical residues of NOD2 involved in muramyl dipeptide recognition. EMBO J. 23, 1587-1597.

van Duist, M.M., Albrecht, M., Podswiadek, M., Giachino, D., Lengauer, T., Punzi, L., and De Marchi, M. (2005). A new CARD15 mutation in Blau syndrome. Eur. J. Hum. Genet. 13, 742–747.

Yu, J.-W., Wu, J., Zhang, Z., Datta, P., Ibrahimi, I., Taniguchi, S., Sagara, J., Fernandes-Alnemri, T. And Alnemri, E.S. (2006). Cryopyrin and pyrin activate caspase-1, but not NF-κB, via ASC oligomerization. Cell Death Differ. 13, 236-249.

Supplemental Figures

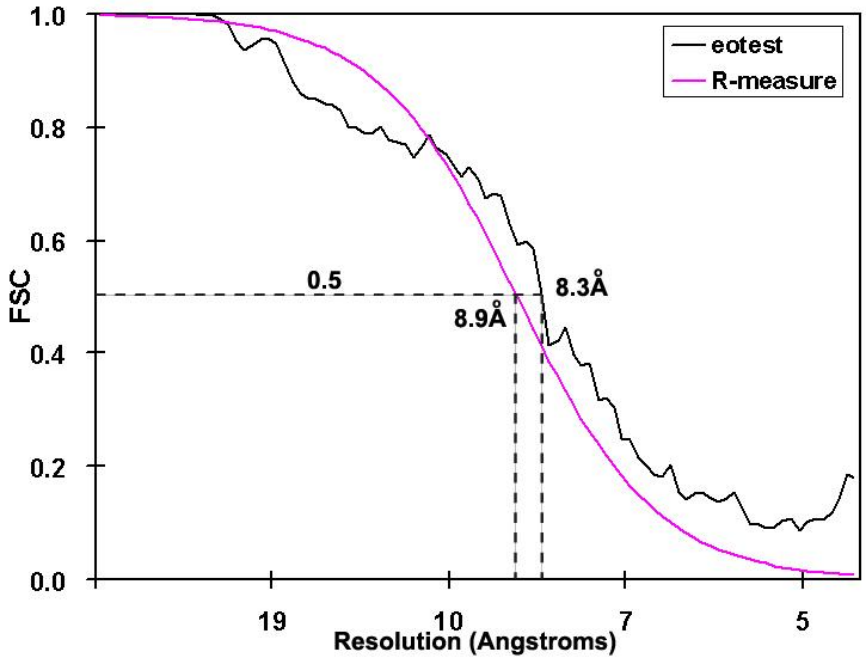

Figure S1. FSC and R-measure curves for the apoptosome-pc-9 CARD complex.

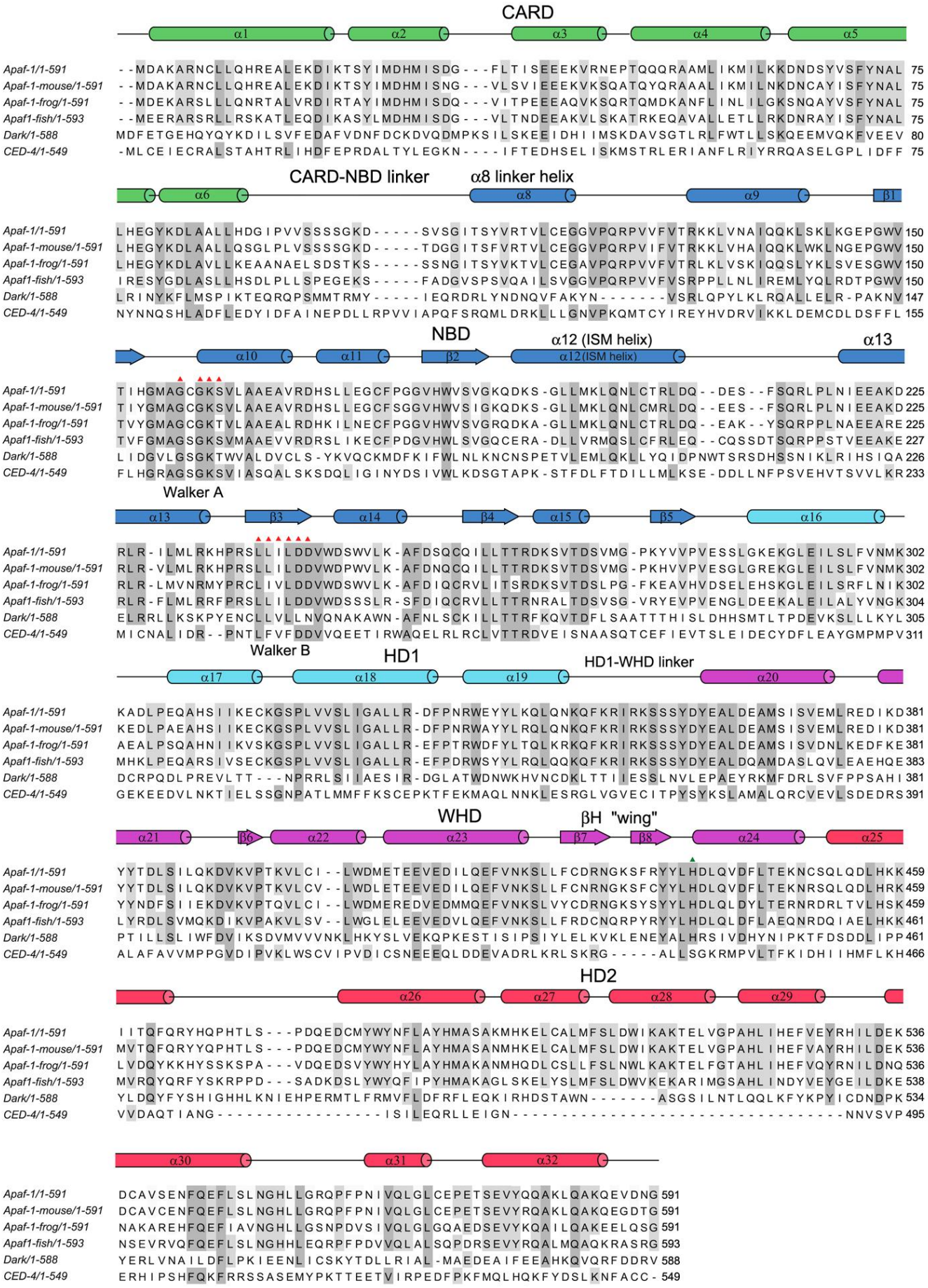
CARD
α1
α2
α3
α4
α5
CARD-NBD linker
α8 linker helix
α6
α8
α9
β1
NBD
α12 (ISM helix)
α13
α10
α11
β2
α12(ISM helix)
Walker A
α13
β3
α14
β4
α15
β5
α16
Walker B
HD1
HD1-WHD linker
α17
α18
α19
α20
WHD
βH "wing"
α21
β6
α22
α23
β7
β8
α24
α25
HD2
α26
α27
α28
α29
α30
α31
α32
Apaf-1/1-591
Apaf-1-mouse/1-591
Apaf-1-frog/1-591
Apaf1-fish/1-593
Dark/1-588
CED-4/1-549

Figure S2. Sequence alignment and structural elements of Apaf-1 and related proteins. This figure has up-dated from a similar figure in Riedl et al., (2005). Walker motif residues are indicated by red triangles and the motifs and domains are labeled.

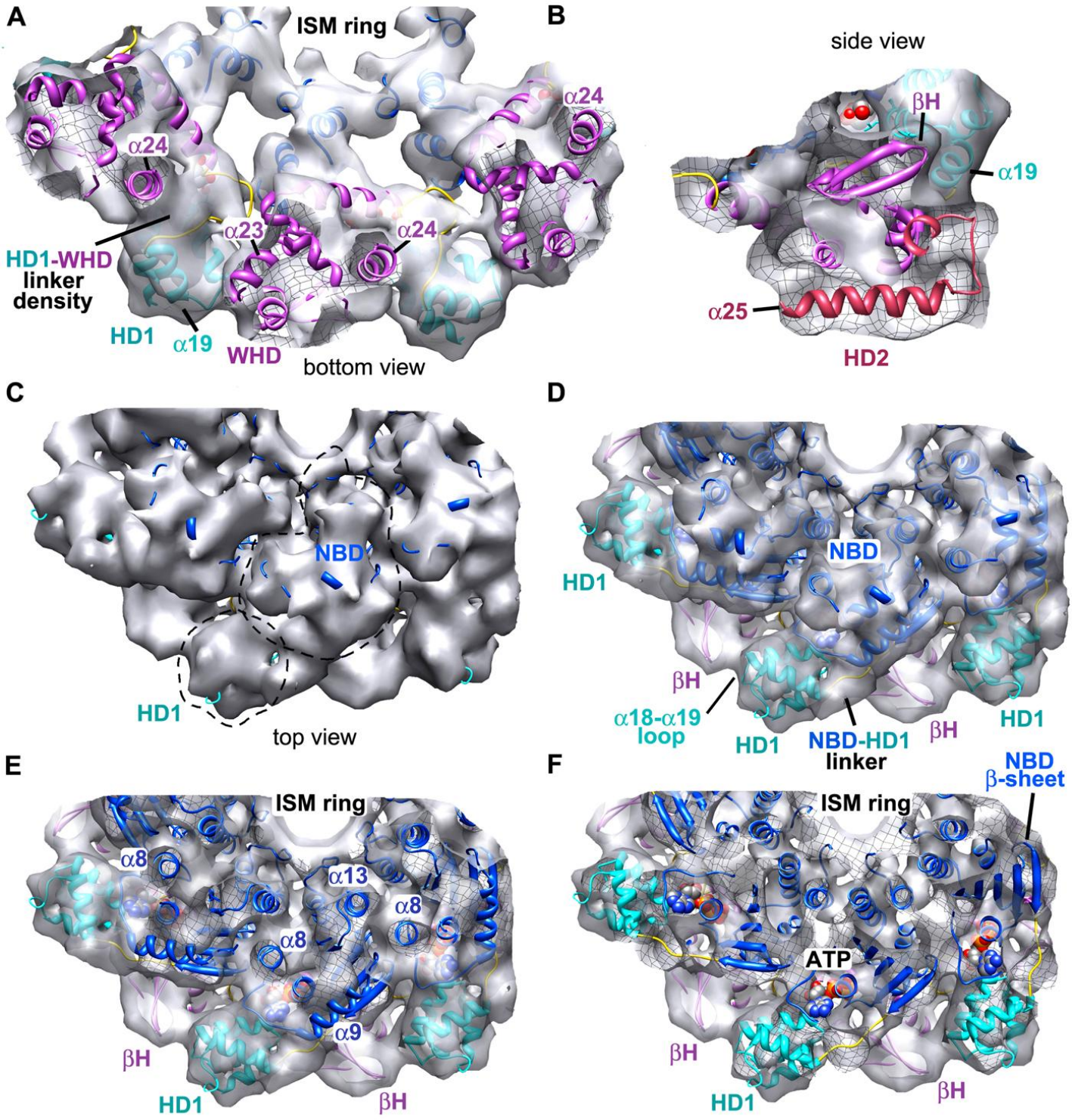

Figure S3. Docking NBD, HD1 and WHD within the central hub.
A. A bottom view is shown of the WHD-HD1 region of the central hub. The fit is quite good as seen in semi-transparent and slabbed views. Density for the HD1-WHD linker is indicated. A black mesh is displayed on the inside of the iso-surface to distinguish it from the outer surface.
B. The fit of the model is shown for a rotated view of the WHD-HD1 region. In this side view, the β7-β8 hairpin "wing" (βH) which gives the WHD its name is shown within density along with helix α25 from HD2. **C.** A top view is shown of the central hub which contains density from 3 Apaf-1 subunits. The positions of NBD and HD1 are indicated with dashed outlines.
D. A similar view to panel C is shown, with the map rendered semi-transparent. The overall fit of NBD, HD1 and WHD within the map is apparent including density for the NBD-HD1 linker and β-hairpin (βH) of the WHD. **E.** A similar view to panel D is shown with the top surface removed, to show the fit of helices α8, α9 and α13 from NBDs. **F.** A deeper slab into the map region shows the fit of a central β-sheet of the NBD and reveals a deep pocket for nucleotide. The fit of the 4-helix bundle in HD1 is also shown.

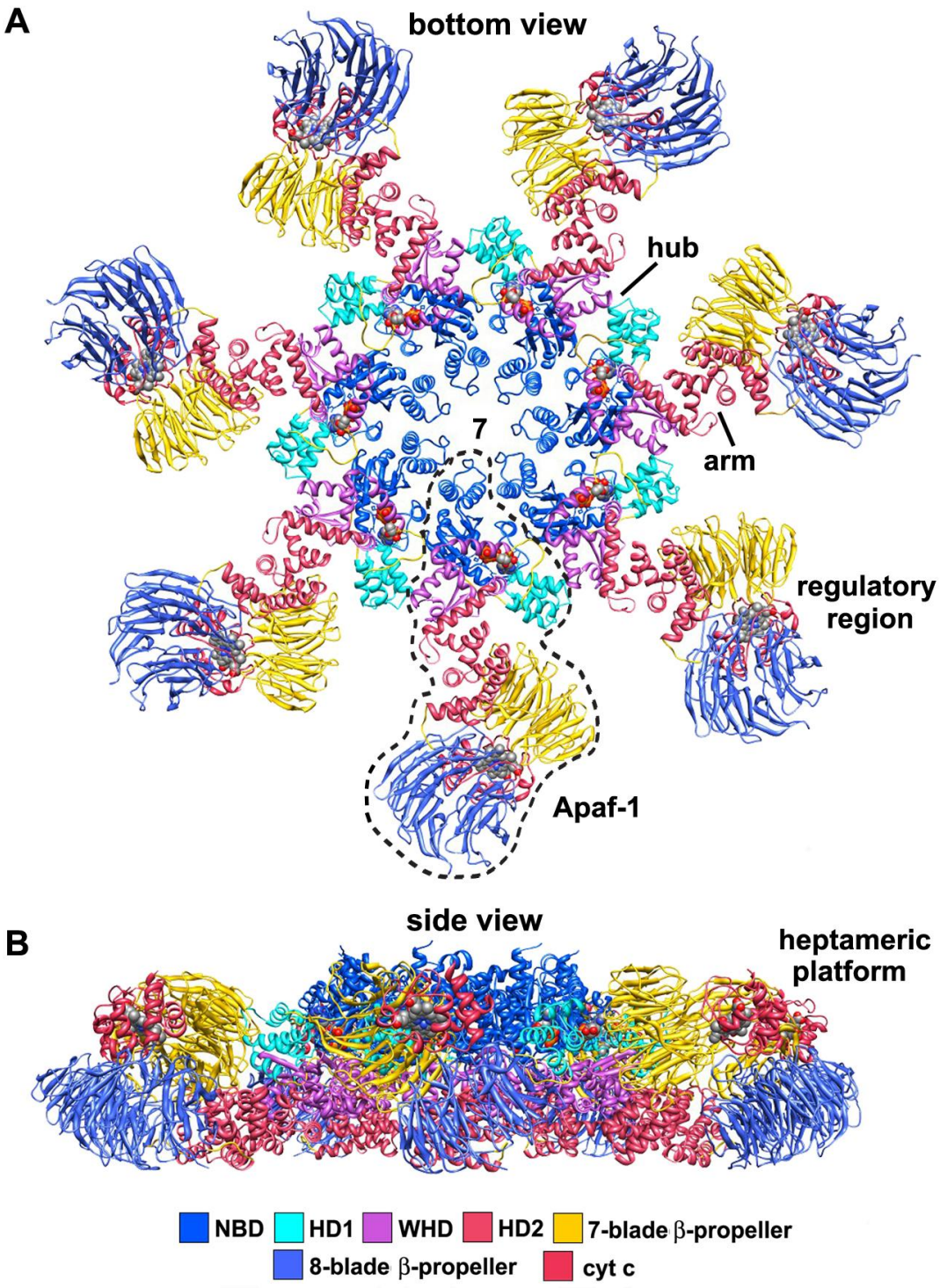

Figure S4. Bottom and side views of the heptameric platform.
A. A molecular model of the platform is shown in a bottom view of the apoptosome. A complete Apaf-1 subunit is outlined by a dashed outline. Nucleotide is bound between the NBD, HD1 and a loop from the α8 linker helix. **B.** The overall dimensions of the platform are ~290 x 75Å in a side view. Flexibly-linked CARDs (not shown) would sit above the central hub in this view.

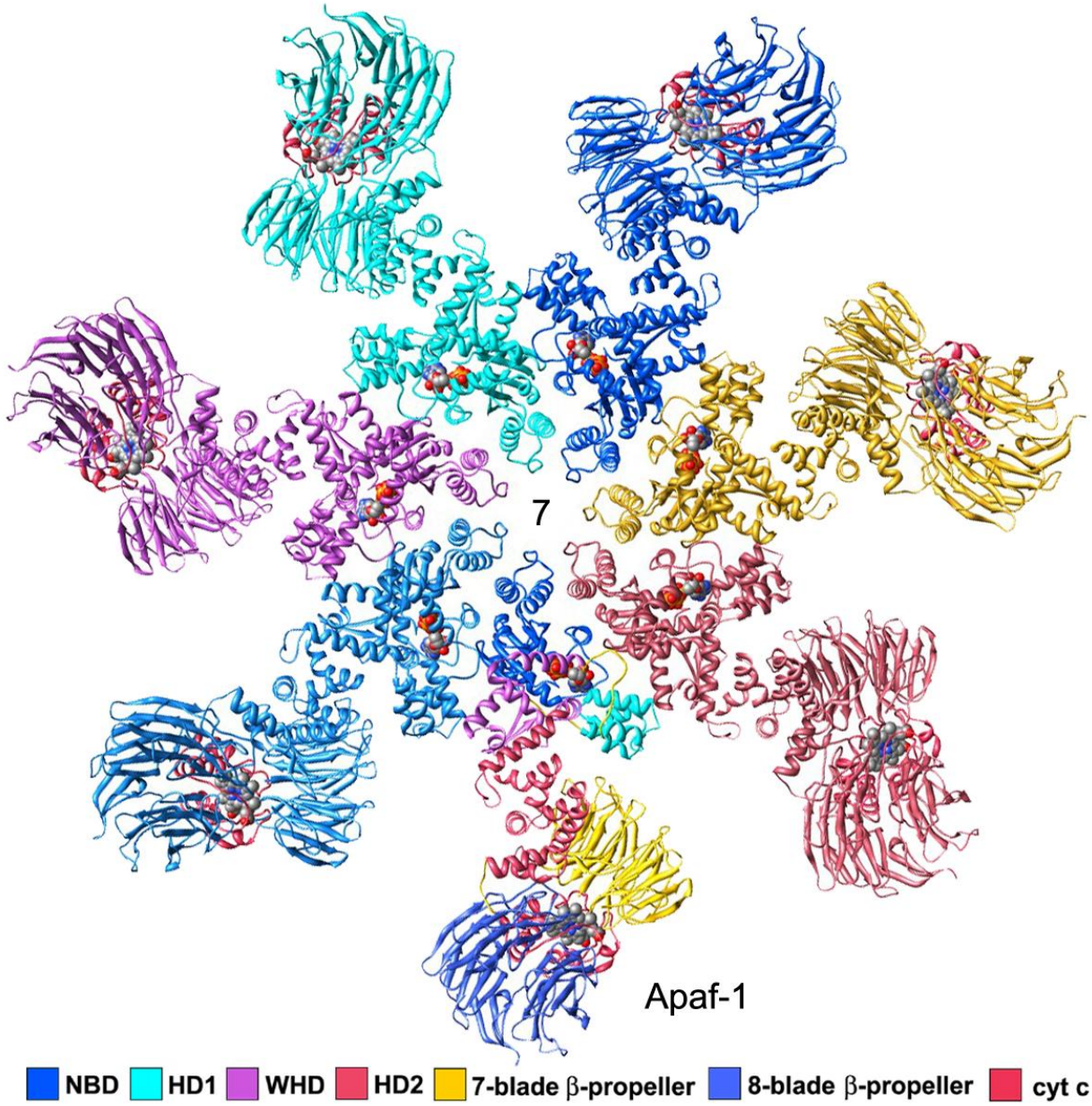

Figure S5. A bottom view of the model reveals subunit boundaries within the apoptosome. Each Apaf-1 subunit has a different color with the exception of the subunit at 6 o'clock which is color coded by domain.

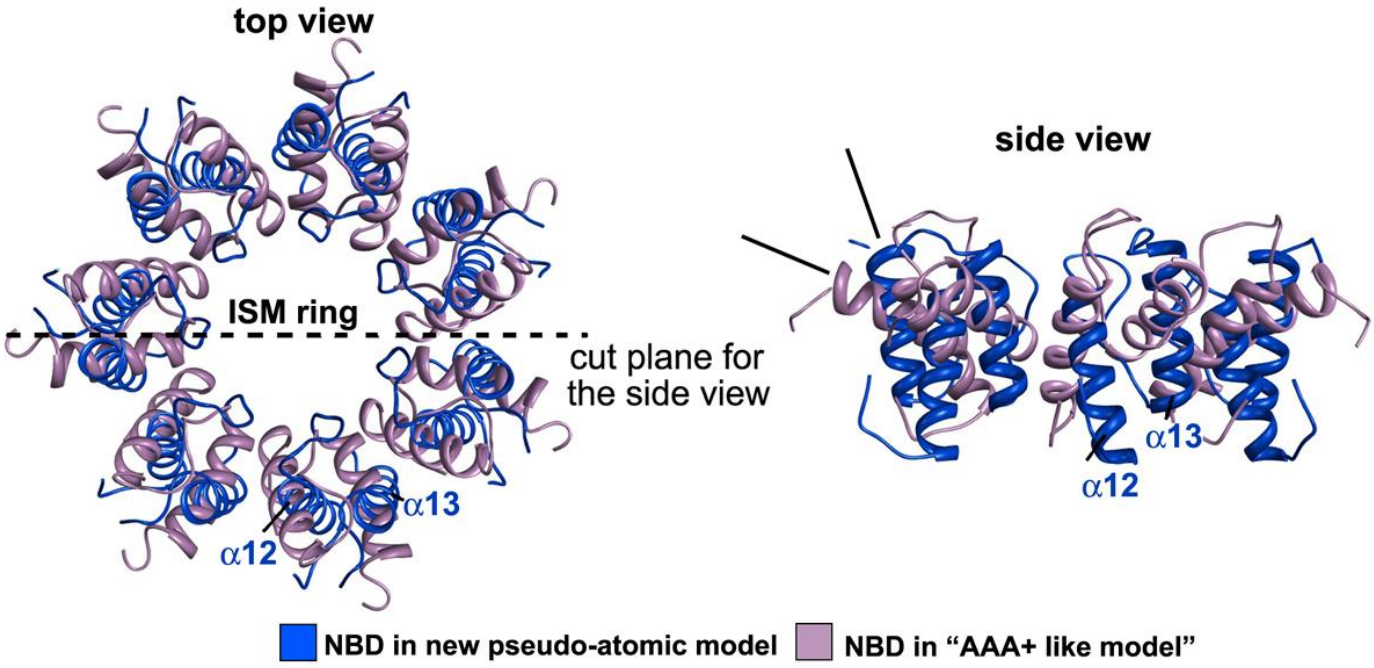

Figure S6. Comparison of models for the ISM ring.

Top and side views are shown for molecular models of the central ISM ring, based on the cryo-EM density map (in blue) and a computational model based on other AAA+ crystal structures (shown in light purple; Diemand and Lupas, 2006). The ISM-α13 ring is aligned nearly vertical along the 7-fold symmetry axis in the cryo-EM density whereas helices in the model show are tilted by ~50-60° from the vertical (see lines).

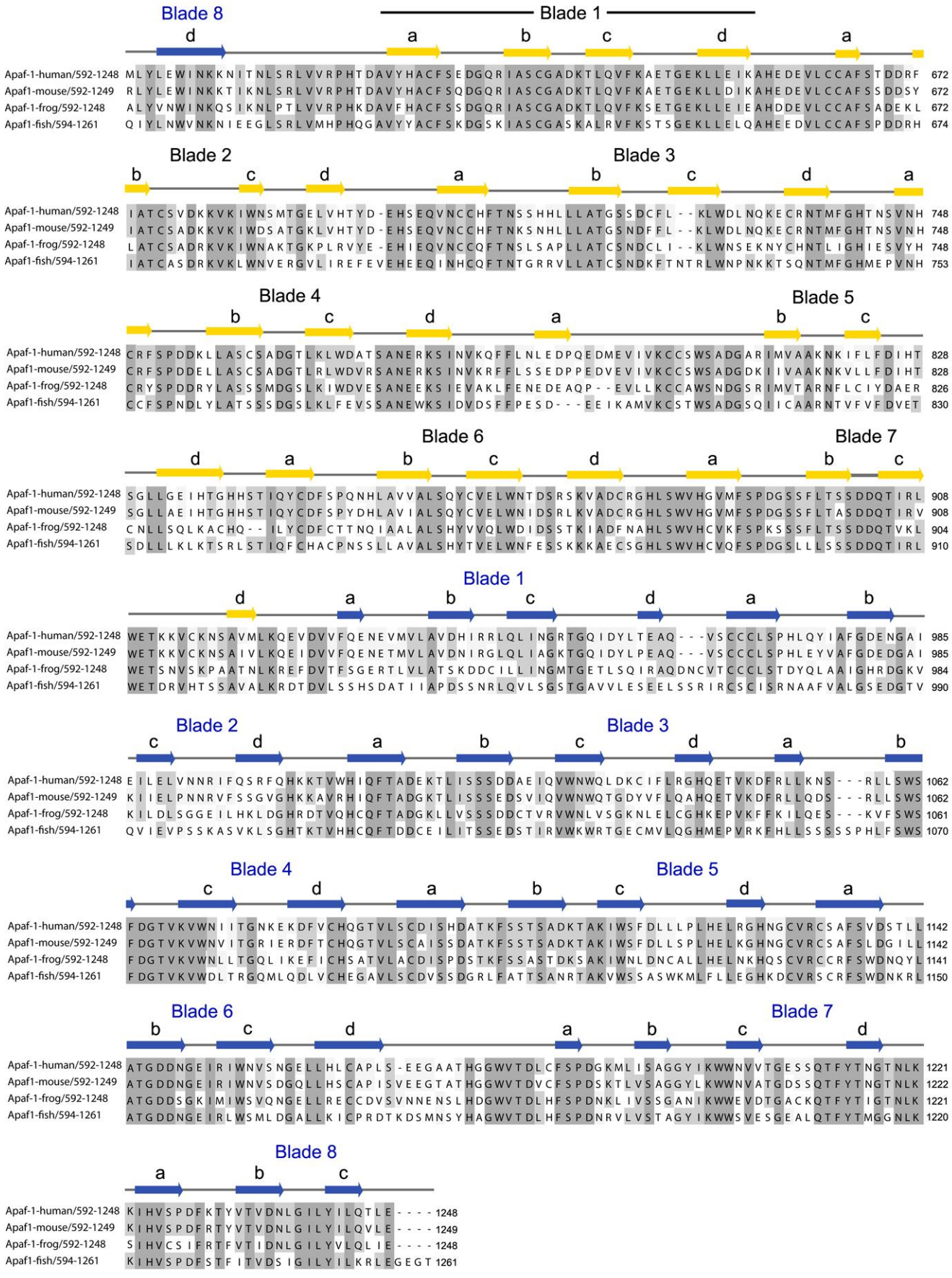
Blade 8
Blade 1
d a b c d a
Apaf-1-human/592-1248 MLYLEWINKKNITNLSRLVVRPHTDAVYHACFSEDGQRIASCGADKTLQVFKAETGEKLLEIKAHEDEVLCCAFSTDDRF 672
Apaf1-mouse/592-1249 RLYLEWINKKTIKNLSRLVVRPHTDAVYHACFSQDGQRIASCGADKTLQVFKAETGEKLLDIKAHEDEVLCCAFSSDDSY 672
Apaf-1-frog/592-1248 ALYVNWINKQSIKNLPTLVVRPHKDAVFHACFSSDGQRIASCGADKTLQVFKSETGEKLLEIEAHDDEVLCCAFSADEKL 672
Apaf1-fish/594-1261 QIYLNWVNKNIEEGLSRLVMHPHQGAVYYACFSKDGSKIASCGASKALRVFKSTSGEKLLELQAHEEDVLCCAFSPDDRH 674
Blade 2
Blade 3
b c d a b c d a
Apaf-1-human/592-1248 IATCSVDKKVKIWNSMTGELVHTYD-EHSEQVNCCHFTNSSHHLLLATGSSDCFL--KLWDLNQKECRNTMFGHTNSVNH 748
Apaf1-mouse/592-1249 IATCSADKKVKIWDSATGKLVHTYD-EHSEQVNCCHFTNKSNHLLLATGSNDFFL--KLWDLNQKECRNTMFGHTNSVNH 748
Apaf-1-frog/592-1248 LATCSADRKVKIWNAKTGKPLRVYE-EHIEQVNCCQFTNSLSAPLLATCSNDCLI--KLWNSEKNYCHNTLIGHIESVYH 748
Apaf1-fish/594-1261 IATCASDRKVKLWNVERGVLIREFEVEHEEQINHCQFTNTGRRVLLATCSNDKFTNTRLWNPNKKTSQNTMFGHMEPVNH 753
Blade 4
Blade 5
b c d a b c
Apaf-1-human/592-1248 CRFSPDDKLLASCSADGTLKLWDATSANERKSINVKQFFLNLEDPQEDMEVIVKCCSWSADGARIMVAAKNKIFLFDIHT 828
Apaf1-mouse/592-1249 CRFSPDDELLASCSADGTLRLWDVRSANERKSINVKRFFLSSEDPPEDVEVIVKCCSWSADGDKIIVAAKNKVLLFDIHT 828
Apaf-1-frog/592-1248 CRYSPDDRYLASSSMDGSLKIWDVESANEEKSIEVAKLFENEDEAQP--EVLLKCCAWSNDGSRIMVTARNFLCIYDAER 826
Apaf1-fish/594-1261 CCFSPNDLYLATSSSDGSLKLFEVSSANEWKSIDVDSFFPESD---EEIKAMVKCSTWSADGSQIICAARNTVFVFDVET 830
Blade 6
Blade 7
d a b c d a b c
Apaf-1-human/592-1248 SGLLGEIHTGHHSTIQYCDFSPQNHLAVVALSQYCVELWNTDSRSKVADCRGHLSWVHGVMFSPDGSSFLTSSDDQTIRL 908
Apaf1-mouse/592-1249 SGLLAEIHTGHHSTIQYCDFSPYDHLAVIALSQYCVELWNIDSRLKVADCRGHLSWVHGVMFSPDGSSFLTASDDQTIRV 908
Apaf-1-frog/592-1248 CNLLSQLKACHQ--ILYCDFCTTNQIAALALSHYVVQLWDIDSSTKIADFNAHLSWVHCVKFSPKSSSFLTSSDDQTVKL 904
Apaf1-fish/594-1261 SDLLLKLKTSRLSTIQFCHACPNSSLLAVALSHYTVELWNFESSKKKAECSGHLSWVHCVQFSPDGSLLLSSSDDQTIRL 910
Blade 1
d a b c d a b
Apaf-1-human/592-1248 WETKKVCKNSAVMLKQEVDVVFQENEVMVLAVDHIRRLQLINGRTGQIDYLTEAQ---VSCCCLSPHLQYIAFGDENGAI 985
Apaf1-mouse/592-1249 WETKKVCKNSAIVLKQEIDVVFQENETMVLAVDNIRGLQLIAGKTGQIDYLPEAQ---VSCCCLSPHLEYVAFGDEDGAI 985
Apaf-1-frog/592-1248 WETSNVSKPAATNLKREFDVTFSGERTLVLATSKDDCILLINGMTGETLSQIRAQDNCVTCCCLSTDYQLAAIGHRDGKV 984
Apaf1-fish/594-1261 WETDRVHTSSAVALKRDTDVLSSHSDATIIAPDSSNRLQVLSGSTGAVVLESEELSSRIRCSCISRNAAFVALGSEDGTV 990
Blade 2
Blade 3
c d a b c d a b
Apaf-1-human/592-1248 EILELVNNRIFQSRFQHKKTVWHIQFTADEKTLISSSDDAEIQVWNWQLDKCIFLRGHQETVKDFRLLKNS---RLLSWS 1062
Apaf1-mouse/592-1249 KIIELPNNRVFSSGVGHKKAVRHIQFTADGKTLISSSEDSVIQVWNWQTGDYVFLQAHQETVKDFRLLQDS---RLLSWS 1062
Apaf-1-frog/592-1248 KILDLSGGEILHKLDGHRDTVQHCQFTADGKLLVSSSDDCTVRVWNLVSGKNLELCGHKEPVKFFKILQES---KVFSWS 1061
Apaf1-fish/594-1261 QVIEVPSSKASVKLSGHTKTVHHCQFTDDCEILITSSEDSTIRVWKWRTGECMVLQGHMEPVRKFHLLSSSSSPHLFSWS 1070
Blade 4
Blade 5
c d a b c d a
Apaf-1-human/592-1248 FDGTVKVWNIITGNKEKDFVCHQGTVLSCDISHDATKFSSTSADKTAKIWSFDLLLPLHELRGHNGCVRCSAFSVDSTLL 1142
Apaf1-mouse/592-1249 FDGTVKVWNVITGRIERDFTCHQGTVLSCAISSDATKFSSTSADKTAKIWSFDLLSPLHELKGHNGCVRCSAFSLDGILL 1142
Apaf-1-frog/592-1248 FDGTVKVWNLLTGQLIKEFICHSATVLACDISPDSTKFSSASTDKSAKIWNLDNCALLHELNKHQSCVRCCRFSWDNQYL 1141
Apaf1-fish/594-1261 FDGTVKVWDLTRGQMLQDLVCHEGAVLSCDVSSDGRLFATTSANRTAKVWSSASWKMLFLLEGHKDCVRSCRFSWDNKRL 1150
Blade 6
Blade 7
b c d a b c d
Apaf-1-human/592-1248 ATGDDNGEIRIWNVSNGELLHLCAPLS-EEGAATHGGWVTDLCFSPDGKMLISAGGYIKWWNVVTGESSQTFYTNGTNLK 1221
Apaf1-mouse/592-1249 ATGDDNGEIRIWNVSDGQLLHSCAPISVEEGTATHGGWVTDVCFSPDSKTLVSAGGYLKWWNVATGDSSQTFYTNGTNLK 1222
Apaf-1-frog/592-1248 ATGDDSGKIMIWSVQNGELLRECCDVSVNNENSLHDGWVTDLHFSPDNKLIVSSGANIKWWEVDTGACKQTFYTIGTNLK 1221
Apaf1-fish/594-1261 ATGDDNGEIRLWSMLDGALLKICPRDTKDSMNSYHAGWVTDLHFSPDNRVLVSTAGYIKWWSVESGEALQTFYTMGGNLK 1220
Blade 8
a b c
Apaf-1-human/592-1248 KIHVSPDFKTYVTVDNLGILYILQTLE---- 1248
Apaf1-mouse/592-1249 KIHVSPDFRTYVTVDNLGILYILQVLE---- 1249
Apaf-1-frog/592-1248 SIHVCSIFRTFVTIDNLGILYVLQLIE---- 1248
Apaf1-fish/594-1261 KIHVSPDFSTFITVDSIGILYILKRLEGEGT 1261

Figure S7. Sequence alignment and structure predication for 7- and 8-blade β-propellers.

Blades and individual β-strands are indicated. The HD2 linker is predicted to form the d-strand in the last blade of the 8-blade β-propeller before continuing on to form the 7-blade propeller and the rest of the 8-blade propeller.

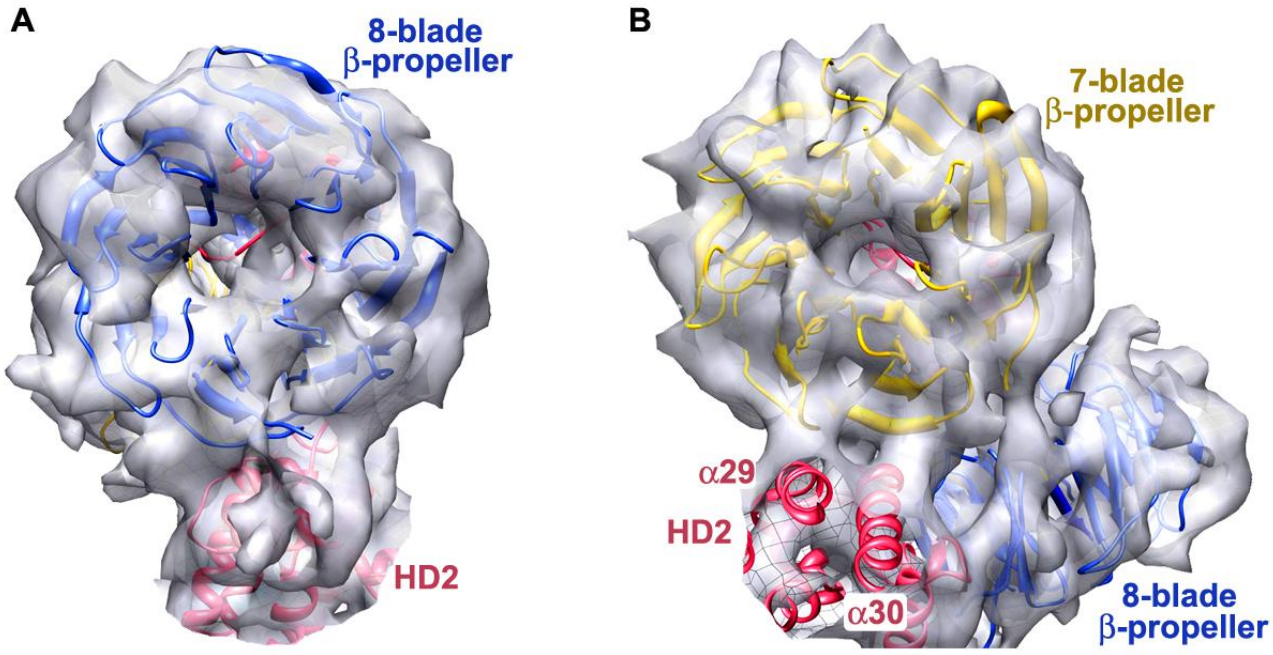

Figure S8. The fit of 7- and 8-blade β-propellers is shown within the regulatory region of the map. HD2 α-helices are also labeled.

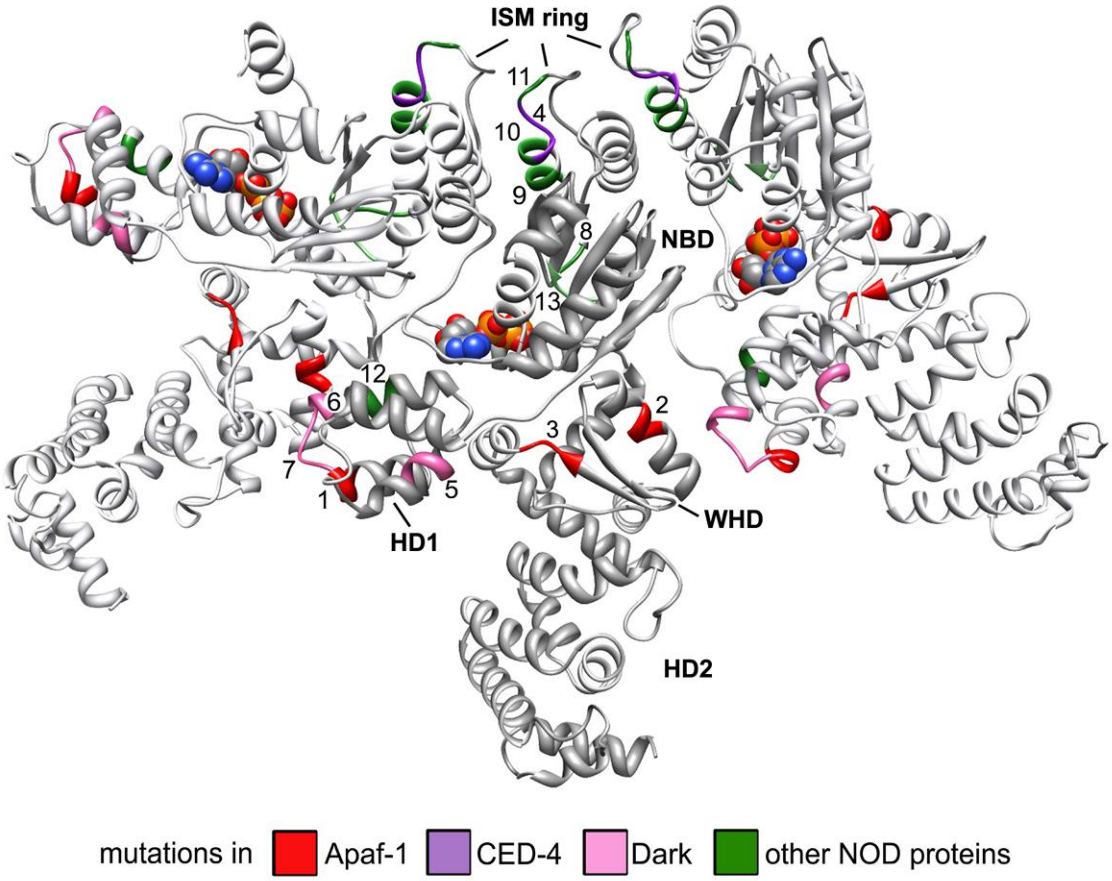

Figure S9. NOD mutations from Apaf-1, Dark, CED4 and other NOD proteins mapped onto the Apaf-1 hub based on sequence alignments.